MOEM

Modern Electronic Materials 2024; 10(1): 3–10
DOI 10.3897/j.moem.10.1.122043

Research Article

Comparison of the structure and physicochemical properties of ZrO_2 based crystals partially stabilized with Y_2O_3, Gd_2O_3 and Sm_2O_3

Artem S. Chislov[1], Mikhail A. Borik[1], Aleksey V. Kulebyakin[1], Elena E. Lomonova[1], Filipp O. Milovich[1], Valentina A. Myzina[1], Aleksey A. Reu[1], Polina A. Ryabochkina[1], Natalya V. Sidorova[2], Nataliya Yu. Tabachkova[1]

1 Prokhorov General Physics Institute of the Russian Academy of Sciences, 38 Vavilov Str., Moscow 119991, Russian Federation

2 Ogarev Mordovia State University, 68/1 Bolshevistskaya Str., Saransk, Republic of Mordovia 430005, Russian Federation

Corresponding author: Artem S. Chislov (chislov.artem@bk.ru)

Received 2 February 2024 ♦ **Accepted** 29 February 2024 ♦ **Published** 3 April 2024

Citation: Chislov AS, Borik MA, Kulebyakin AV, Lomonova EE, Milovich FO, Myzina VA, Reu AA, Ryabochkina PA, Sidorova NV, Tabachkova NYu (2024) Comparison of the structure and physicochemical properties of ZrO_2 based crystals partially stabilized with Y_2O_3, Gd_2O_3 and Sm_2O_3. *Modern Electronic Materials* 10(1): 3–10. https://doi.org/10.3897/j.moem.10.1.122043

Abstract

The phase composition, density, microhardness and fracture toughness of $(ZrO_2)_{1-x}(R_2O_3)_x$ crystals (where R = Y, Sm and Gd) for x = 0.02–0.04 have been compared. The crystals have been grown using directional melt crystallization in a cold crucible. The phase composition of the crystals has been studied using X-ray diffraction and Raman spectroscopy. The microhardness and fracture toughness of the crystals have been evaluated by means of indentation. At stabilizing oxide concentrations of ≥ 2.8 mol.% for Y_2O_3 and Gd_2O_3 and ≥ 3.7 mol.% for Sm_2O_3 the crystals have densities close to the theoretical ones and contain two tetragonal phases. At lower stabilizing oxide concentrations the crystals contain the monoclinic phase. The fracture toughness of the tetragonal crystals increases with the ionic radius of the stabilizer. The highest fracture toughness values achieved when stabilized by a specific oxide are 11.0, 13.0 and 14.3 MPa·m$^{1/2}$ for the 2.8YSZ, 2.8GdSZ and 3.7SmSZ crystals, respectively. The fracture toughness proves to depend on the crystallographic orientation of the crystals. The results of this work can be used in the design and fabrication of various structural components and devices.

Keywords

directional crystallization, growth from melt, partially stabilized zirconia, toughness

1. Introduction

Zirconia based solid solutions deliver a unique combination of chemical, optical, mechanical, thermophysical and electrical properties which determine their widespread applications in biomedical, structural, heat-insulating, optical and tribotechnical materials [1–6].

Pure ZrO_2 has three polymorphic modifications at normal pressure: monoclinic, tetragonal and cubic, with only the former one being stable at room temperature. The high-temperature cubic and tetragonal modifications are stabilized by zirconia doping with alkaline-earth or rare-earth element oxides [1]. Depending on their structure, these materials can be conditionally divided in two

major types, i.e., fully and partially stabilized zirconia (FSZ and PSZ, respectively). FSZ have single-phase cubic structures. PSZ contain monoclinic and/or tetragonal phases since the quantity of the stabilizing oxide is insufficient to fully stabilize the cubic phase. A more detailed classification of PSZ ceramics has been suggested [7] according to which of greatest interest are poly- and single crystal structures consisting of the tetragonal phase.

These tetragonal solid solutions are distinguished by a combination of good mechanical and tribological parameters with chemical and biological inertness, low heat conductivity and high thermal expansion coefficient and therefore attract great attention of researchers [8–11]. Tetragonal ZrO_2 solid solution ceramics and crystals currently are widely used in the fabrication of friction parts (plugs, valves, bearings, pistons etc.) [12], thermal barrier coatings [13], mill rollers, wire drawing dies [14], dental and biomedical prosthetics [3], and surgical scalpels [15].

A distinctive feature of the tetragonal solid solutions is a high fracture toughness combined with a high mechanical strength. The high fracture toughness of these materials originates from the so-called transformation hardening [16, 17]. Efficient transformation hardening requires the retention of the maximum possible quantity of the tetragonal ZrO_2 phase, with its optimum transformability at specific temperatures [14, 18]. The term "transformability" is usually treated as the capability of the tetragonal ZrO_2 phase of a phase transformation to the monoclinic ZrO_2 phase due to mechanical stress at crack tips.

The metastability of the tetragonal phase which largely determines its transformability depends on the concentration and type of the stabilizing oxide used. Stabilizing oxides can be, e.g., yttria and oxides of alkaline-earth and rare-earth elements. The most studied ZrO_2 solid solutions containing 3 mol.% Y_2O_3 exhibit high bending strengths (800–1200 MPa) and microhardness (11–13 GPa), but only moderate fracture toughness (~6 MPa·$m^{1/2}$) [9, 19]. Various oxides were used as stabilizers, e.g. Yb_2O_3 [20], Gd_2O_3 [21], CeO_2 [22, 23], Er_2O_3 [24] and Dy_2O_3 [25]. However, those works are few and their results are difficult for analysis since almost all the studies were carried out for ceramic specimens differing in phase composition, microstructure, and grain size and preheating history. The listed factors exert a great effect on the properties of the material, including the mechanical ones. It is of interest to compare the structure and mechanical properties of ZrO_2 based solid solutions partially stabilized with Y_2O_3 and other rare-earth element oxides synthesized using the same method and with similar temperature and time synthesis parameters. This will clarify the effect of trivalent cation ionic radius on the properties and structure formation in ZrO_2 based tetragonal solid solutions. Such a study would be of great practical interest since its results could be used for designing high performance construction materials.

The use of directional melt crystallization allows growing crystals without grain structures and grain boundaries thus eliminating the effect of microstructure-related factors on the properties of the materials. Moreover, studies of single crystals reveal the anisotropy of their mechanical properties which is a difficult task for isotropic ceramic specimens. Studies of the anisotropy of mechanical properties allow fabricating single crystal products with preset crystallographic orientations for which the fracture toughness and/or strength is the highest. ZrO_2 based single crystal solid solutions stabilized with various oxides were obtained using this method earlier [26–27].

This work reports a comparative study of the phase composition and mechanical properties of partially stabilized zirconia synthesized using directional melt crystallization. Gd_2O_3 and Sm_2O_3 were chosen as rare-earth element oxides since the ionic radii of Gd^{3+} and Sm^{3+} are greater than that of Y^{3+}. The ionic radii of Y, Gd and Sm oxides change in the following sequence: $R_{Y^{3+}}$ = 0.1019 nm < $R_{Gd^{3+}}$ = 0.1053 nm < $R_{Sm^{3+}}$ = 0.1074 nm. This work is a continuation of our earlier study [28] dealing with the structural and electrical properties of crystals with close compositions which were considered as potential materials for solid electrolytes having oxygen ion conductivity.

2. Materials and methods

The crystals were grown using directional melt crystallization in a water-cooled 100 mm diam. crucible by direct induction heating. This growth method was described in detail elsewhere [29]. The crystals were grown out on a "Kristall-407" high frequency growth installation in air. The power source was a 63 kW power 5.28 MHz high-frequency generator. The raw powders of ZrO_2, Y_2O_3, Gd_2O_3 and Sm_2O_3 (with at least 99.99 % main substance content, Russia) were preliminarily mechanically mixed in the required proportions in an attritor and loaded into the crucible. The charge weight was 4.5–5 kg. Melting was initiated using zirconium. After melting of the whole raw powder mixture the melt was held in air for 30 min. The melt was then crystallized by moving the crucible out of the heated zone at 10 mm/h speed. The cross-section and length of the as-grown crystals were 5–20 mm and 30–40 mm, respectively.

The density of the specimens was measured by hydrostatic weighing on a Sartorius hydrostatic weighing device; the measurement error being 0.1%.

The phase composition of the crystals was studied using X-ray diffraction with a Bruker D8 instrument in CuK_α radiation. The diffractometer operation mode was 40 кV @ 40 mA. The study was conducted using the conventional method for single crystals. The as-grown crystals had no predominant crystallographic orientations. Therefore, each crystal was preliminarily oriented along specific crystallographic directions in the diffractometer. Wafers for the studies were cut from the middle parts of the crystals. The phase composition of the crystals was studied for wafers cut from the crystals perpendicular to the <100> direction. The 2θ/ω-mode scanning range

was 20 to 140 arc deg with 0.02 arc deg steps. The {100} planes of the multiphase composition crystals exhibited several simultaneous reflections from a single cut that were produced by different phases, these reflections being split at high 2θ (~130 arc deg). The phase fractions were determined from the diffraction peak intensities normalized to the integral reflection coefficients of the phases.

Local phase analysis in the vicinity of indentations was carried out using Raman spectroscopy in the 50–1400 cm^{-1} wavenumber range under a Renishaw inVia Raman confocal microscope. A 532 nm laser was used as an excitation source. The laser focus point was chosen using a built-in optical microscope (×20). The focused beam diameter on the sample was ~1 μm. For Raman spectra recording, the laser radiation power was set to 100 mW, the signal accumulation time being 5 seconds. The rate of the tetragonal-to-monoclinic phase transition (R_m) was calculated from the Raman band intensity ratio for the monoclinic and tetragonal phases using the following formula [30]:

$$R_m = \frac{I^m_{178} + I^m_{190}}{I^t_{146} + I^m_{178} + I^m_{190}}. \quad (1)$$

For mechanical studies, 5 mm thick plates were cut from the crystals and then grinded and polished. The specimens were grinded with α-SiC (M10) suspension. ACM3/2 or ACM2/1 diamond pastes were used for polishing. Chemomechanical polishing was used at the final stage for damaged surface layer removal. The polishing agents were compositions of nanometer-sized amorphous silica particles. The chemomechanical polishing time was 30–60 min. The roughness of the as-polished surfaces was 0.3–0.5, and the surfaces contained no microscratches and were leveled and smooth.

The microhardness and fracture toughness of the crystals were measured via indentation on the {001} plane at different specimen rotation angles in their planes. Anisotropy was measured in the 0–90 arc deg specimen rotation angular range with 22.5 arc deg steps, the 0 arc deg position corresponding to the <100> direction. The instruments used were a DM 8BAUTO microhardness tester with a Vickers indenter (maximum load 20 N) and a Wolpert Hardness Tester 930 with a minimum load of 50 N. The microhardness and fracture toughness were measured at 5 and 100 N loads, respectively, with 10 s dwell times. The indentation spacing was 400 mm. A total of 25 indentations were made for each crystallographic direction.

The fracture toughness (K_{1C}) was calculated using the Niihara formula for the Palmqvist Crack system as reported earlier [31–33]:

$$K_{1C} = 0.035(L/a)^{-1/2}(CE/H)^{2/5}\, Ha^{1/2}C^{-1}, \quad (2)$$

where K_{1C} is the stress intensity coefficient (MPa·$m^{1/2}$); L is the radial crack length (m); a is the indentation half-width (m); C is the constraint factor (= 3); E is Young's modulus (= 250 Pa); H is the microhardness (Pa).

The K_{1C} parameter was calculated for radial cracks around indentations if the crack length met the criterion ($0.25 \le l/a \le 2.5$) for Palmqvist cracks.

3. Results and discussion

The test materials were $(ZrO_2)_{1-x}(R_2O_3)_x$ crystals (where R = Y, Sm and Gd) for x = 0.02; 0.028; 0.032; 0.037 and 0.04, synthesized using directional melt crystallization under similar temperature and time conditions. The use

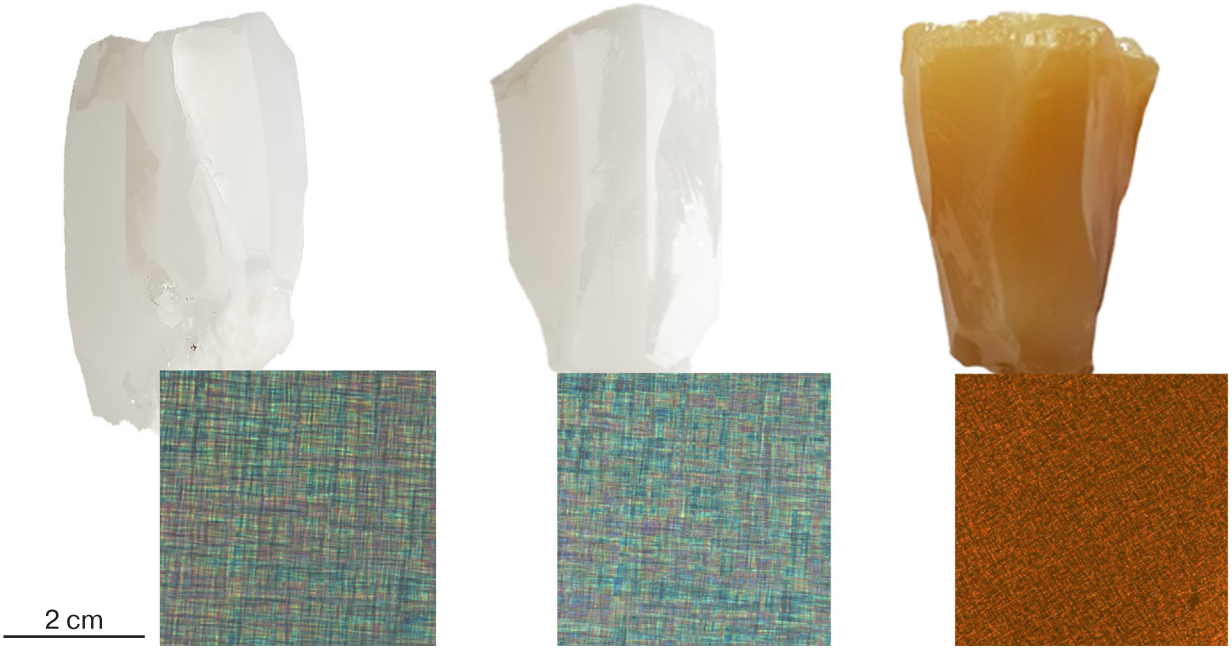

Figure 1. Appearance of crystals. *Inserts:* optical images in transmitted polarized light of the samples microstructure

of similar synthesis conditions justifies comparative analyses of crystal parameters for similar stabilizing oxide-concentrations. Hereinafter, the crystals will be denoted as *x*YSZ, *x*GdSZ and *x*SmSZ where *x* is the concentration of Y_2O_3, Gd_2O_3 and Sm_2O_3 stabilizing oxides in mol.%, respectively. Figure 1 shows the appearance of the crystals and optical images of the microstructure of samples made from crystals.

The densities of the crystals partially stabilized with Y_2O_3, Gd_2O_3 and Sm_2O_3 were measured. The densities of the tetragonal crystals were close to their theoretical values. This indicates the absence of defects in the form of pores and microcracks. Figure 2 shows crystal density as a function of the type and concentration of stabilizing oxide.

With an increase in the concentration of stabilizing oxide from 2.0 to 2.8 mol.% for YSZ and GdSZ and from 2.0 to 3.7 mol.% for SmSZ the experimentally measured densities of the crystals increase, this being mainly accounted for by a decrease in the content of the monoclinic phase the density of which is lower than that of the tetragonal phase. With further increases in the stabilizing oxide concentration the densities of the GdSZ and SmSZ crystals increase whereas that of the YSZ crystal decreases. This is caused by the fact that, unlike the Y atoms which are lighter than the Zr ones, the Sm and Gd atoms are heavier than the Zr ones. The density of the tetragonal crystals (at stabilizing oxide concentrations of $\geq$ 3.7 mol.%) for comparable concentrations increases in the sequence Y $\rightarrow$ Sm $\rightarrow$ Gd, in agreement with the atomic weights of the respective elements.

A disruption in the monotonic pattern of the crystal density *vs* concentration function can serve as an indicator of changes in the phase composition of the crystals and hence can be used for finding a lower concentration limit of tetragonal structure stabilization in the crystals.

Table 1 summarizes data on the phase composition, phase weight fractions and tetragonality degrees of $(ZrO_2)_{1-x}(Y_2O_3)_x$, $(ZrO_2)_{1-x}(Gd_2O_3)_x$ and $(ZrO_2)_{1-x}(Sm_2O_3)_x$ solid solutions for *x* from 0.02 to 0.04.

At the lowest stabilizing oxide concentration which is 2.0 mol.% all the test crystals contained the monoclinic phase. The concentration limits at which the monoclinic phase was not observed were 2.8, 2.8 and 3.7 mol.% for Y_2O_3, Gd_2O_3 and Sm_2O_3 stabilizing oxides, respectively.

At stabilizing oxide concentrations of $\geq$ 2.8 mol.% for Y_2O_3 and Gd_2O_3 and $\geq$ 3.7 mol.% for Sm_2O_3 the crystals contain two tetragonal phases having different tetragonality degrees. Thus, for Sm_2O_3 stabilizing oxide the tetragonal phaseis stabilized in the whole crystal bulk at a higher stabilizing oxide concentration.

An increase in the stabilizing oxide concentration in the tetragonal crystals causes a decline in the quantity of the transformable tetragonal phase (*t*) and an increase in the quantity of the non-transformable tetragonal phase (*t*′), the tetragonality degrees ($c/\sqrt{2}a$) of these phases decreasing with an increase in the stabilizing oxide concentration.

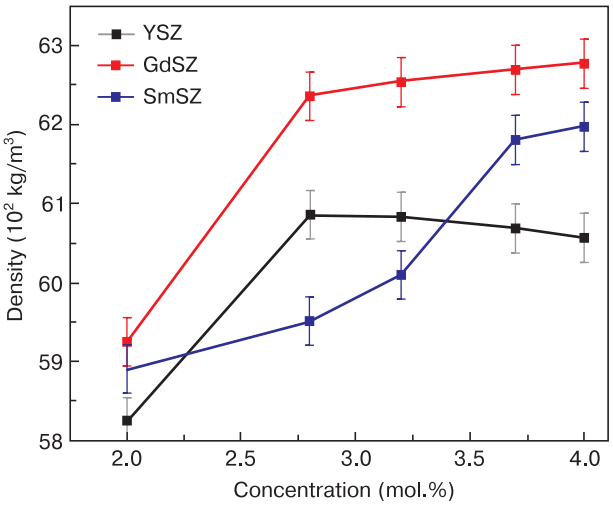

Figure 2. Crystal density as a function of type and concentration of stabilizing oxide

Table 1. Phase composition, phase weight fractions and tetragonality degrees of $(ZrO_2)_{1-x}(R_2O_3)_x$ solid solutions (where *R* = Y, Sm and Gd) for *x* = 0.02; 0.028; 0.032; 0.037; 0.04

x (mol.%)	YSZ			GdSZ			SmSZ		
	Phase	wt.%	$c/\sqrt{2}a$	Phase	wt.%	$c/\sqrt{2}a$	Phase	wt.%	$c/\sqrt{2}a$
2.0	*m*	75(5)	1.0164	*m*	85(5)	1.0170	*m*	100(5)	–
	t	25(5)		*t*	15(5)				
2.8	*t*	87(5)	1.0152	*t*	90(5)	1.0162	*t*	40(5)	1.0720
	t′	13(5)	1.0054	*t*`	10(5)	1.0053	*m*	60(5)	
3.2	*t*	78(5)	1.0147	*t*	84(5)	1.0159	*t*	65(5)	1.0710
	t′	22(5)	1.0052	*t*`	16(5)	1.0047	*t*′	10(5)	1.0036
							m	25(5)	
3.7	*t*	70(5)	1.0145	*t*	77(5)	1.0154	*t*	85(5)	1.0167
	t′	30(5)	1.0050	*t*`	23(5)	1.0040	*t*′	15(5)	1.0035
4.0	*t*	62(5)	1.0143	*t*	72(5)	1.0151	*t*	76(5)	1.0165
	t′	38(5)	1.0049	*t*`	28(5)	1.0037	*t*′	24(5)	1.0034

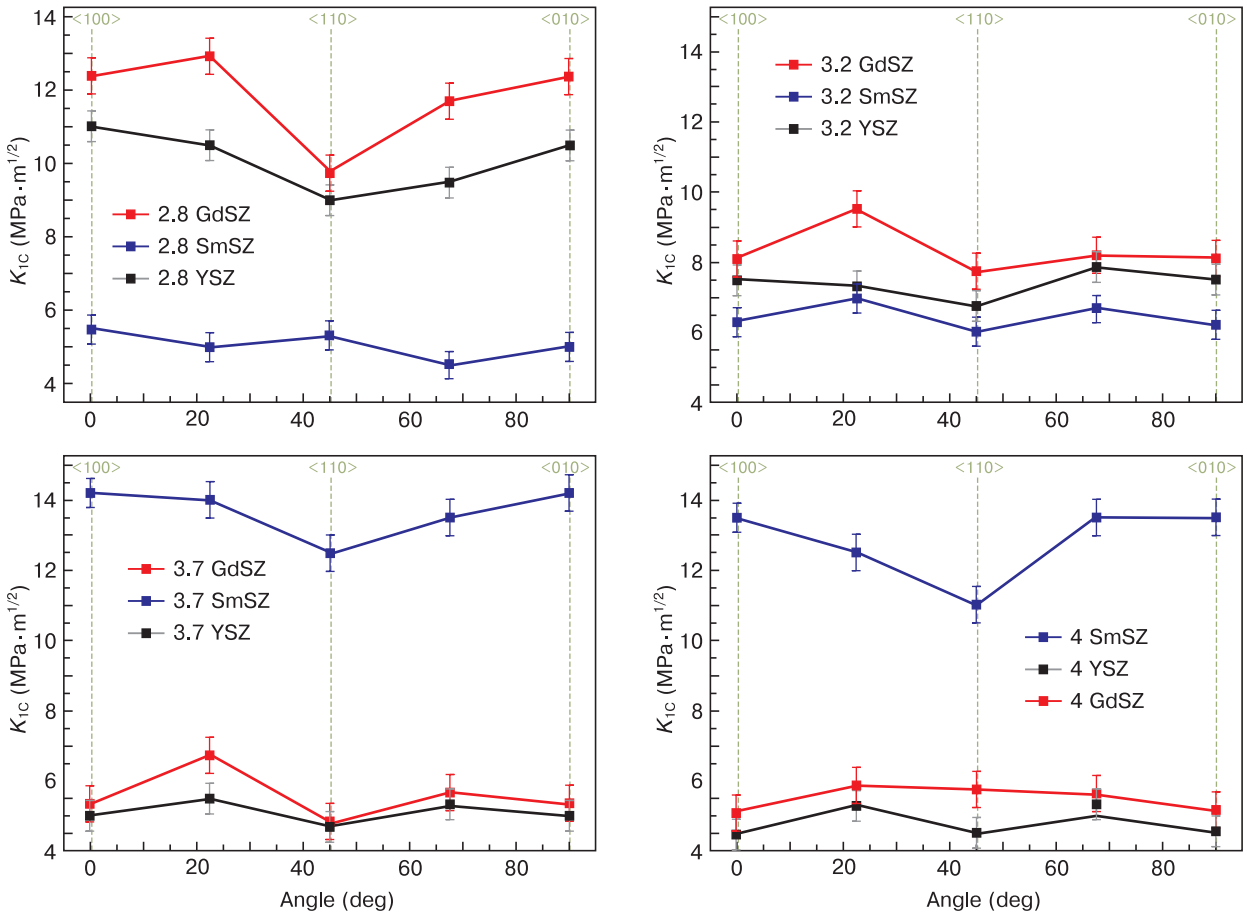

Figure 3. Fracture toughness measured in the {100} plane for different angles of indenter diagonal relative to the <100> direction in specimen plane for YSZ, GdSZ and SmSZ crystals

To discuss the phase composition data for the crystals we analyze the ZrO_2–Y_2O_3 binary system phase diagram fragment for the 2–4 mol.% Y_2O_3 concentration range [34]. The phase diagrams of the ZrO_2–Gd_2O_3 and ZrO_2–Sm_2O_3 systems in the composition region of interest differ but slightly in the concentration and temperature boundaries of cubic, tetragonal and monoclinic phase existence regions [35]. In accordance with the phase diagram, cubic crystals grow at the crystallization temperature and their cooling triggers a phase transition from the single-phase cubic region to the two-phase ($c + t$) region. During this transition, there is no decomposition into equilibrium c and t phases. At the critical overcooling for a specific composition, a first-order transition occurs that is accompanied by stabilizing oxide redistribution and the formation of two metastable tetragonal phases with compositions within the two-phase region near its equilibrium boundaries. Further crystal cooling to below 1200 °C does not change the compositions of the two metastable tetragonal phases since the cation diffusion rate in that temperature range is very low [36]. A synchrotron study of the phase composition of the ceramic ZrO_2 specimens stabilized with (2–4) mol.% Y_2O_3 revealed two tetragonal phases with different tetragonality degrees and Y_2O_3 contents [37]. A formula was suggested for the calculation of rare-earth stabilizing oxide concentration in the tetragonal phases based on the phase tetragonality degrees [38]. In accordance with that formula, an increase in the tetragonality degree indicates a decrease in the stabilizing oxide content in the tetragonal phases. The data summarized in Table 1 suggest that the solid solutions stabilized with large-radius trivalent cations are susceptible to more effective phase decomposition. In other words, the larger the trivalent cation radius, the closer the tetragonality degrees of the t and t' phases are to the parameters of the equilibrium t and c phases, which are 1.022 [39] and 1.0, respectively. This result is in agreement with other data [25] indicating that the width of the two-phase ($c + t$) region depends on cation type and increases for large-radius cations. The proximity of the metastable t phase to the $t/(c + t)$ phase boundary facilitates the stress-induced $t \rightarrow m$ phase transition and hence increases the transformability of the material.

Table 2 presents the experimental microhardness data for the YSZ, GdSZ and SmSZ crystals. No microhardness anisotropy was observed in the {100} plane for different crystallographic orientations of the indenter diagonals.

For all the test compositions, an increase in the stabilizing oxide concentration leads to an increase in the microhardness. The observed microhardness behavior regularities depending on stabilizing oxide ionic radius agree with earlier data [28]. Microhardness can depend

Table 2. Microhardness of YSZ, GdSZ and SmSZ crystals

Concentration (mol.%)	Y_2O_3	Gd_2O_3	Sm_2O_3
	HV (GPa)		
2.0	10.4 ± 0.4	9.0 ± 0.4	8.6 ± 0.4
2.8	12.9 ± 0.4	12.5 ± 0.4	8.8 ± 0.4
3.2	13.0 ± 0.4	12.6 ± 0.4	10.8 ± 0.4
3.7	13.6 ± 0.4	12.8 ± 0.4	11.3 ± 0.4
4.0	13.9 ± 0.4	13.4 ± 0.4	12.2 ± 0.4

not only on stabilizing oxide ionic radius but also on phase composition. For example, the solid solutions containing the monoclinic phase have the lowest microhardness. Furthermore, as follows from Table 1, an increase in the stabilizing oxide concentration leads to an increase in the fraction of the t' phase which has a close to cubic structure and hence exhibits a higher microhardness [40].

Recommended fracture toughness test methods for ceramic and brittle materials are single edge v-notched beam (SEVNB), chevron-notched beam (CNB), single-edge pre-cracked beam (SEPB) and surface crack in flexure (SCF) [41]. In this work, the fracture toughness was tested using the indentation method which is widely used for ZrO_2 based ceramic toughness testing [19]. Unlike for recommended conventional fracture toughness testing methods, cracks propagate in a high-gradient stress field; however, proper and careful use of this method yields reproducible data [33].

Figure 3 shows the experimental data on the fracture toughness of the YSZ, GdSZ and SmSZ crystals of different compositions for different indenter diagonal orientations in the specimen plane. The measurements were made for wafers cut from the crystals perpendicular to the <100> direction.

The fracture toughness is the highest among the Y_2O_3, Gd_2O_3 and Sm_2O_3 stabilized crystals for the 2.8YSZ, 2.8GdSZ and 3.7SmSZ solid solutions, respectively. The crystals containing 3.7 mol.% Sm_2O_3 have the highest K_{1C} (14.3 MPa·m$^{1/2}$) among all the test crystals. The fracture toughness values for the 2.8YSZ and 2.8GdSZ crystals were 11.0 and 13.0 MPa·m$^{1/2}$, respectively. All these compositions exhibited clear K_{1C} anisotropy, with K_{1C} being the lowest for the <110> indenter diagonal orientation. K_{1C} of the YSZ and GdSZ crystals decreased with an increase in the stabilizing oxide concentration, and their anisotropy became less expressed. Of the Sm_2O_3 stabilized crystals studied, those containing 2.8 and 3.2 mol.% Sm_2O_3, in which the monoclinic phase was found, had the lowest K_{1C}.

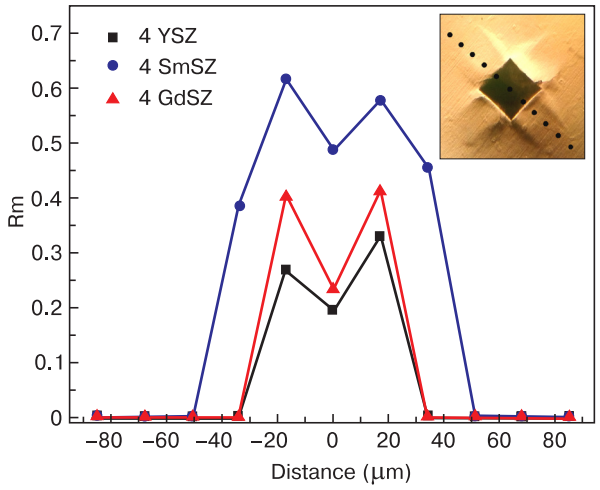

Figure 4. Tetragonal-to-monoclinic phase transition rate for 4.0YSZ, 4.0GdSZ and 4.0SmSZ crystals in local areas near indentations. *Inset:* indentation images with Raman spectra recording points marked

Note that the highest K_{1C} regardless of stabilizing oxide type were observed at the lowest concentrations that are required for tetragonal phase stabilization and complete monoclinic phase suppression. These boundary concentrations are controlled not only by the type of the stabilizing oxide but also by the methods and conditions of solid solution synthesis. It should also be noted that the increase of K_{1C} in the sequence 2.8YSZ → 2.8GdSZ → 3.7SmSZ can be attributed to an increase in the transformability of the material due to an increase in the tetragonality degree of the transformable phase ($c/\sqrt{2}a$ = 1.0152, 1.0162 and 1.0167 for 2.8YSZ, 2.8GdSZ and 3.7SmSZ, respectively). An increase in the fracture toughness with an increase in the rare-earth cation radius was also observed for 3.5 mol.% RE_2O_3 (RE = Dy, Y, Er, Yb) stabilized ZrO_2 [25].

The contribution of the transformation hardening mechanism to the increase in the fracture toughness was theoretically estimated on the basis of micromechanical models in accordance with the following equation [42]:

$$\Delta K_C = \frac{0.38 f E \varepsilon \sqrt{h}}{(1-\nu)}, \quad (3)$$

where f is the volume fraction of the tetragonal phase that is transformable in the transformation zone, E is the elastic modulus of the material, ε is the volume deformation involved in the transformation, h is the width of the transformation zone and ν is Poisson's ratio.

Equation (3) suggests that an increase in the content of the transformable phase and enlargement of the transformation zone should increase the fracture toughness of the material.

One can hypothesize that the width of the transformation zone is proportional to the width of the monoclinic phase zone around the indentation. Figure 4 shows rate of the tetragonal-to-monoclinic phase transition for the 4.0YSZ, 4.0GdSZ and 4.0SmSZ crystals in local areas near indentations.

As follows from Fig. 4, the $t \rightarrow m$ phase transition region of the 4.0YSZ and 4.0GdSZ crystals is almost completely within the indentation limits, whereas for the 4.0SmSZ crystal it is noticeably wider. Moreover, the R_m parameter in the latter case is also higher than those for the 4.0YSZ and 4.0GdSZ crystals. Thus, the indentation-induced $t \rightarrow m$ phase transition in the 4.0SmSZ

crystals is more intense and occurs in a greater volume. Both those factors determine the extremely high fracture toughness of the 4.0SmSZ crystals.

Thus, analysis of the experimental data presented above suggests that the ionic radii of stabilizing oxides affect the mechanical parameters of the crystals in an indirect manner, more specifically, via the specific features of phase formation and changes of phase ratios in the test solid solutions.

4. Conclusion

The phase composition, density, microhardness and fracture toughness of $(ZrO_2)_{1-x}(R_2O_3)_x$ (R = Y, Gd, Sm) solid solution crystals for x = 0.02–0.04 were compared. The highest fracture toughness figures were 11.0, 13.0 and 14.3 MPa·m$^{1/2}$ for the 2.8YSZ, 2.8GdSZ and 3.7SmSZ crystals, respectively. All the high-K_{1C} crystals contained two tetragonal phases differing in the chemical compositions. The fracture toughness of the tetragonal crystals increased with the trivalent cation ionic radius due to an increase in the transformability of the metastable t phase. The crystals having fracture toughness values of above ~10.0 MPa·m$^{1/2}$ exhibited clear anisotropy. K_{1C} for the <100> direction were ~20% higher than those for the <110> direction.

Analysis of the results obtained suggests that the ionic radii of stabilizing oxide cations affect the mechanical parameters of the crystals in an indirect manner, more specifically, via the specific features of phase formation and changes in the phase ratios of the test solid solutions.

Acknowledgements

This research was funded by the Russian Science Foundation, Grant No. 22-29-01220.

References

1. Chevalier J., Gremillard L., Virkar A.V., Clarke D.R. The tetragonal-monoclinic transformation in zirconia: lessons learned and future trends. *Journal of the American Ceramic Society*. 2009; 92(9): 1901–1920. https://doi.org/10.1111/j.1551-2916.2009.03278.x
2. Huang X., Zakurdaev A., Wang D. Microstructure and phase transformation of zirconia-based ternary oxides for thermal barrier coating applications. *Journal of Materials Science*. 2008; 8: 2631–2641. https://doi.org/10.1007/s10853-008-2480-x
3. Piconi C., Maccauro G. Zirconia as a ceramic biomaterial. *Biomaterials*. 1999; 20(1): 1–25. https://doi.org/10.1016/S0142-9612(98)00010-6
4. Kelly J.R., Denry I. Stabilized zirconia as a structural ceramic: an overview. *Dental Materials*. 2008; 24(3): 289–298. https://doi.org/10.1016/j.dental.2007.05.005
5. Vaßen R., Jarligo M.O., Steinke T., Mack D.E., Stöver D. Overview on advanced thermal barrier coatings. *Surface and Coatings Technology*. 2010; 205(4): 938–942. https://doi.org/10.1016/j.surfcoat.2010.08.151
6. Badwal S.P.S. Zirconia-based solid electrolytes: microstructure, stability and ionic conductivity. *Solid State Ionics*. 1992; 52(1-3): 23–32. https://doi.org/10.1016/0167-2738(92)90088-7
7. Claussen N. Microstructural design of zirconia-toughened ceramics (ZTC). In: N. Claussen, M. Ruhle, A.H. Heuer (Eds.). Science and technology of zirconia II. Columbus, OH: American Ceramic Society; 1984. P. 325–351.
8. Li Q., Hao X., Gui Y., Qiu H., Ling Y., Zheng H., Omran M., Gao L., Chen J., Chen G. Controlled sintering and phase transformation of yttria-doped tetragonal zirconia polycrystal material. *Ceramics International*. 2021; 47(19): 27188–27194. https://doi.org/10.1016/j.ceramint.2021.06.139
9. Chevalier J., Liens A., Reveron H., Zhang F., Reynaud P., Douillard T., Preiss L., Sergo V., Lughi V., Swain M., Courtois N. Forty years after the promise of «ceramic steel?»: Zirconia-based composites with a metal-like mechanical behavior. *Journal of the American Ceramic Society*. 2020; 103(3): 1482–1513. https://doi.org/10.1111/jace.16903
10. Merk A.-L., Kern F. Influence of starting powder choice on structure property relations in gadolinia stabilized zirconia 3Gd-TZP manufactured from co-milled starting powders. *Journal of the European Ceramic Society*. 2021; 41(15): 7783–7791. https://doi.org/10.1016/j.jeurceramsoc.2021.08.002
11. Zhang F., Batuk M., Hadermann J., Manfredi G., Mariën A., Vanmeensel K., Inokoshi M., van Meerbeek B., Naert I., Vleugels J. Effect of cation dopant radius on the hydrothermal stability of tetragonal zirconia: Grain boundary segregation and oxygen vacancy annihilation. *Acta Materialia*. 2016; 106: 48–58. https://doi.org/10.1016/j.actamat.2015.12.051
12. Qi B., Liang S., Li Y., Zhou C., Yu H., Li J. ZrO_2 matrix toughened ceramic material-strength and toughness. *Advanced Engineering Materials*. 2022; 24(6): 2101278. https://doi.org/10.1002/adem.202101278
13. Padture N.P., Gell M., Jordan E.H. Thermal barrier coatings for gas-turbine engine applications. *Science*. 2002; 296(5566): 280–284. https://doi.org/10.1126/science.1068609
14. Hannink R.H.J., Kelly P.M., Muddle B.C. Transformation toughening in zirconia-containing ceramics. *Journal of the American Ceramic Society*. 2000; 83(3): 461–487. https://doi.org/10.1111/j.1151-2916.1987.tb04865.x
15. Belov S.V., Borik M.A., Danileiko J.K., Shulutko A.M., Lomonova E.E., Osiko V.V., Salyuk V.A. New bipolar electrosurgical tools based on zirconia. *Biomedical Engineering*. 2013; 47(2): 78–82. https://doi.org/10.1007/s10527-013-9339-4
16. Heuer A.H., Rühle M., Marshall D.B. On the thermoelastic martensitic transformation in tetragonal zirconia. *Journal of the*

American Ceramic Society. 1990; 73(4): 1084–1093. https://doi.org/10.1111/j.1151-2916.1990.tb05161.x

17. Garvie R.C., Hannink R.H.J., Pascoe R.T. Ceramic Steel? *Nature*. 1975; 258: 703–704. https://doi.org/10.1038/258703a0
18. Basu B. Toughening of yttria-stabilised tetragonal zirconia ceramics. *International Materials Reviews*. 2005; 50(4): 239–256. https://doi.org/10.1179/174328005X41113
19. Eichler J., Rödel J., Eisele U., Hoffman M. Effect of grain size on mechanical properties of submicrometer 3Y-TZP: fracture strength and hydrothermal degradation. *Journal of the American Ceramic Society*. 2007; 90(9): 2830–2836. https://doi.org/10.1111/j.1551-2916.2007.01643.x
20. Kern F., Gadow R. Tough to brittle transition with increasing grain size in 3Yb-TZP ceramics manufactured from stabilizer coated nanopowder. *Journal of the Ceramic Society of Japan*. 2016; 124(10): 1083–1089. https://doi.org/10.2109/jcersj2.16106
21. Bhattacharyya S., Agrawal D.C. Microstructure and mechanical properties of ZrO_2–Gd_2O_3 tetragonal polycrystals. *Journal of Materials Science*. 2002; 37: 1387–1394. https://doi.org/10.1023/A:1014572629824
22. Zang S., He N., Sun X., Sun M., Wu W., Yang H. Influence of additives on the purity of tetragonal phase and grain size of ceria-stabilized tetragonal zirconia polycrystals (Ce-TZP). *Ceramics International*. 2019; 45(1): 394–400. https://doi.org/10.1016/j.ceramint.2018.09.179
23. Yuan Z., Vleugels J., van der Biest O. Synthesis and characterization of CeO_2-coated ZrO_2 powder-based TZP. *Materials Letters*. 2000; 46(5): 249–254. https://doi.org/10.1016/S0167-577X(00)00180-4
24. Duran P., Recio P., Jurado J.R., Pascual C., Moure C. Preparation, sintering, and properties of translucent Er_2O_3-doped tetragonal zirconia. *Journal of the American Ceramic Society*. 1989; 72(11): 2088–2093. https://doi.org/10.1111/j.1151-2916.1989.tb06036.x
25. Guo L., Li M., Zhang C., Huang X., Ye F., Dy_2O_3 stabilized ZrO_2 as a toughening agent for $Gd_2Zr_2O_7$ ceramic. *Materials Letters*. 2017; 188: 142–144. https://doi.org/10.1016/j.matlet.2016.11.038
26. Borik M.A., Bublik V.T., Kulebyakin A.V., Lomonova E.E., Milovich F.O., Myzina V.A., Osiko V.V., Seryakov S.V., Tabachkova N.Y. Change in the phase composition, structure and mechanical properties of directed melt crystallised partially stabilised zirconia crystals depending on the concentration of Y_2O_3. *Journal of the European Ceramic Society*. 2015; 35(6): 1889–1894. https://doi.org/10.1016/j.jeurceramsoc.2014.12.012
27. Borik M.A., Borichevskij V.P., Bublik V.T., Kulebyakin A.V., Lomonova E.E., Milovich F.O., Myzina V.A., Ryabochkina P.A., Sidorova N.V., Tabachkova N.Yu. Anisotropy of the mechanical properties and features of the tetragonal to monoclinic transition in partially stabilized zirconia crystals. *Journal of Alloys and Compounds*. 2019; 792: 1255–1260. https://doi.org/10.1016/j.jallcom.2019.04.105
28. Agarkov D.A., Borik M.A., Chislov A.S., Komarov B.E., Kulebyakin A.V., Kuritsyna I.E., Lomonova E.E., Milovich F.O., Myzina V.A., Tabachkova N.Yu. Solid electrolytes based on zirconium dioxide partially stabilized with oxides of yttrium, gadolinium, and samarium. *Journal of Solid State Electrochemistry*. 2023. https://doi.org/10.1007/s10008-023-05695-4
29. Osiko V.V., Borik M.A., Lomonova E.E. Synthesis of refractory materials by skull melting technique. In: Springer Handbook of Crystal Growth. Berlin; Heidelberg: Springer-Verlag; 2010. P. 433—477. https://doi.org/10.1007/978-3-540-74761-1_14
30. Chien F.R., Ubic F.J., Prakach V., Heuer A.H. Stress-induced martensitic transformation and ferroelastic deformation adjacent microhardness indents in tetragonal zirconia single crystals. *Acta Materialia*. 1998; 46(6): 2151–2171. https://doi.org/10.1016/S1359-6454(97)00444-8
31. Niihara K. A fracture mechanics analysis of indentation-induced Palmqvist crack in ceramics. *Journal of Materials Science Letters*. 1983; 2(5): 221–223. https://doi.org/10.1007/BF00725625
32. Niihara K., Morena R., Hasselman D.P.H. Evaluation of K_{Ic} of brittle solids by the indentation method with low crack-to-indent ratios. *Journal of Materials Science Letters*. 1982; 1: 13–16. https://doi.org/10.1007/BF00724706
33. Moradkhani A., Baharvandi H. Effects of additive amount, testing method, fabrication process and sintering temperature on the mechanical properties of Al_2O_3/3Y-TZP composites. *Engineering Fracture Mechanics*. 2018; 191: 446–460. https://doi.org/10.1016/j.engfracmech.2017.12.033
34. Scott H.G. Phase relationships in the zirconia-yttria system. *Journal of Materials Science*. 1975; 10: 1527–1535. https://doi.org/10.1007/BF01031853
35. Wang C., Zinkevich M., Aldinger F. Phase diagrams and thermodynamics of rare-earth-doped zirconia ceramics. *Pure and Applied Chemistry*. 2007; 79(10): 1731–1753. https://doi.org/10.1351/pac200779101731
36. Kilo M., Taylor M.A., Argirusis Ch., Borchardt G., Lesage B., Weber S., Scherrer S., Scherrer H., Schroeder M., Martin M. Cation self-diffusion of ^{44}Ca, ^{88}Y and ^{96}Zr in single crystalline calcia- and yttria-doped zirconia. *Journal of Applied Physics*. 2003; 94(12): 7547–7552. https://doi.org/10.1063/1.1628379
37. Yamashita I., Tsukuma K., Tojo T., Kawaji H., Atake T. Synchrotron X-ray study of the crystal structure and hydrothermal degradation of yttria-stabilized tetragonal zirconia polycrystal. *Journal of the American Ceramic Society*. 2008; 91(5): 1634–1639. https://doi.org/10.1111/j.1551-2916.2007.02191.x
38. Yoshimura M., Yashima M., Noma T., Sōmiya S. Formation of diffusionlessly transformed tetragonal phases by rapid quenching of melts in ZrO_2-$RO_{1.5}$ systems (R = rare earths). *Journal of Materials Science*. 1990; 25: 2011–2016. https://doi.org/10.1007/BF01045757
39. Kisi E.H., Howard C.J. Crystal structures of zirconia phases and their inter-relation. *Key Engineering Materials*. 1998; 153-154: 1–36. https://doi.org/10.4028/www.scientific.net/KEM.153-154.1
40. Lorenzo-Martin C., Ajayi O.O., Singh D., Routbort J.L. Evaluation of scuffing behavior of single-crystal zirconia ceramic materials. *Wear*. 2007; 263(7-12): 872–877. https://doi.org/10.1016/j.wear.2006.12.054
41. Quinn G.D., Bradt R.C. On the Vickers indentation fracture toughness test. *Journal of the American Ceramic Society*. 2007; 90(3): 673–680. https://doi.org/10.1111/j.1551-2916.2006.01482.x
42. Evans A.G., Cannon R.M. Overview no. 48: Toughening of brittle solids by martensitic transformations. *Acta Metallurgica*. 1986; 34(5): 761–800. https://doi.org/10.1016/0001-6160(86)90052-0